

## Article

# Efficient Degradation of Antibiotics by Activating Peroxymonosulfate (PMS) with Biochar (BC)-Modified FeO<sub>x</sub> under UVA-LED Irradiation

Peng Chen <sup>1,†</sup>, Liping Zhang <sup>1,†</sup>, Zhiliang Cheng <sup>1,\*</sup> , Jinshan Tang <sup>1</sup>, Heng Huang <sup>1</sup>, Chengzong Jian <sup>1</sup> and Zejun Wei <sup>2,\*</sup>

<sup>1</sup> School of Chemistry and Chemical Engineering, Chongqing University of Technology, Chongqing 400054, China; ocean954700819@163.com (P.C.); 15923941877@163.com (L.Z.); cqldx1822@163.com (J.T.); 17848668465@163.com (H.H.); chengzjian@163.com (C.J.)

<sup>2</sup> Chongqing Academy of Science and Technology, Chongqing 401123, China

\* Correspondence: purper@cqut.edu.cn (Z.C.); wzj185630@163.com (Z.W.)

<sup>†</sup> These authors contributed equally to this work.

**Abstract:** There are obvious drawbacks for the traditional treatment methods of antibiotics, such as low efficiency and high cost. In this paper, FeO<sub>x</sub> catalysts, modified with the biochar (BC) of maple leaf (FeO<sub>x</sub>@BC), were successfully prepared by the hydrothermal method. Then, the FeO<sub>x</sub>@BC was investigated to activate peroxymonosulfate (PMS) under UVA-LED irradiation for the degradation of tetracycline hydrochloride (TC). Subsequently, the changes in valence states before and after the reaction of ions were investigated by XPS spectra, and the process mechanism was presented. The results demonstrated that the TC degradation efficiency reached 96% in the FeO<sub>x</sub>@BC + PMS + UVA-LED system within 40 min, which was higher than 57% efficiency for the α-Fe<sub>2</sub>O<sub>3</sub> + PMS + UVA-LED system. The electron transfer was promoted in the FeO<sub>x</sub>@BC + PMS + UVA-LED system due to the doping of BC. The Fe(III) was transformed into Fe(II) under UVA-LED irradiation, and Fe(II) activated continuously PMS to generate active oxygen species. Furthermore, it had excellent reusable performance and structural stability, and the degradation efficiency was still as high as 80% after five cycles. It was proved that SO<sub>4</sub><sup>•-</sup>, •OH, O<sub>2</sub><sup>•-</sup> and h<sup>+</sup> participated in the degradation process of TC to different degrees by quenching experiments and EPR tests. In summary, FeO<sub>x</sub>@BC is an inexpensive, reusable and efficient catalyst.

**Keywords:** PMS; Reactive Oxygen Species (ROS); FeO<sub>x</sub>@BC + PMS + UVA-LED system; antibiotics



check for updates

**Citation:** Chen, P.; Zhang, L.; Cheng, Z.; Tang, J.; Huang, H.; Jian, C.; Wei, Z. Efficient Degradation of Antibiotics by Activating Peroxymonosulfate (PMS) with Biochar (BC)-Modified FeO<sub>x</sub> under UVA-LED Irradiation. *Crystals* **2023**, *13*, 1248. <https://doi.org/10.3390/cryst13081248>

Academic Editor: Maria Milanova

Received: 4 July 2023

Revised: 5 August 2023

Accepted: 10 August 2023

Published: 12 August 2023



**Copyright:** © 2023 by the authors. Licensee MDPI, Basel, Switzerland. This article is an open access article distributed under the terms and conditions of the Creative Commons Attribution (CC BY) license (<https://creativecommons.org/licenses/by/4.0/>).

## 1. Introduction

Recently, with the rapid development of medical technology, antibiotics are extensive applications in the treatment of diseases [1]. Tetracycline hydrochloride (TC), as one of the typical antibiotics, is generally used in medical treatment, owing to its low price and good bacteriostatic effect [2,3]. However, only a fraction of antibiotics are absorbed by the body, and the majority of them are excreted through urine and feces. This phenomenon leads to antibiotics entering the aquatic environment and causing pollution. For instance, the concentration of antibiotics in pig farm wastewater and surrounding groundwater is 19.9–416.4 µg/L, and the hospital pharmaceutical wastewater is as high as 100–500 mg/L [4]. Meanwhile, it is difficult to completely degrade due to the complex structure of TC. Consequently, it is an urgent problem for antibiotic wastewater to efficiently and greenly degrade.

Persulfate has received more and more attention in the treatment of organic pollutants because of its uniquely excellent performance. The sulfate radical (SO<sub>4</sub><sup>•-</sup>) produced by persulfate is a powerful oxidant with an oxidation potential of 2.5–3.1 V, and it has high-degradation efficiency (10<sup>6</sup>–10<sup>9</sup> M<sup>-1</sup>·s<sup>-1</sup>) [2,5]. Additionally, the half-life of SO<sub>4</sub><sup>•-</sup> is

30–40  $\mu\text{s}$ , which makes it better able to degrade organic pollutants [6]. Peroxymonosulfate (PMS) is typically used as a reagent for the production of  $\text{SO}_4^{\bullet-}$  thanks to its low price. But the PMS itself is relatively stable, enough to produce  $\text{SO}_4^{\bullet-}$  less efficiently, and other methods are needed to activate it, such as ultraviolet light [7], heat energy [8], ultrasound [9], microwaves [10], photocatalysis [11]. Nevertheless, the traditional physical methods require a higher energy consumption, which also means expensive costs. By contrast, catalysts have received increasing attention from researchers due to their high efficiency and low-cost characteristics. Currently, iron has been evidenced to be a useful way to activate PMS, and has been widely used for its characteristics, including easy availability, non-toxicity and low cost. And coupled with photocatalysis to activate PMS, the Fe(III) to Fe(II) cycle rate can be enhanced, and the reusability of the catalyst can be improved.

Biochar (BC) is usually derived from agriculture and is widely used due to its excellent physical and chemical characteristics, such as sample preparation, abundant resources and low price [12,13]. Specifically, BC has a large specific surface area and porous structure, which means it can provide more active sites. Furthermore, it can participate in electron transfer and redox reactions due to its electronegativity, dispersion and functional group properties [14]. BC can serve as a carrier for active substances due to its excellent characteristics, and its catalytic performance is greatly improved after being combined with iron.

In this paper, the  $\alpha\text{-Fe}_2\text{O}_3$  catalyst was successfully modified by adding BC to prepare the  $\text{FeO}_x\text{@BC}$  catalyst, and the catalyst was used to activate PMS to degrade TC. The morphology and structure of the catalyst were characterized by XRD, FT-IR, UV-vis, BET, SEM and TEM/HRTEM. Meanwhile, different single process parameters, including the mass ratio of Fe to BC, catalyst concentrations, PMS concentrations, initial concentrations of TC, reaction temperatures and initial pHs, were used to evaluate the TC degradation efficiency. The degradation efficiency of coexisting anions and humic acid on TC in the  $\text{FeO}_x\text{@BC} + \text{PMS} + \text{UVA-LED}$  system were also investigated based on the above study. Supplementarily, the reusable performance of the catalyst was researched. Finally, the reaction mechanism was revealed through quenching experiments and EPR tests.

## 2. Experimental

### 2.1. Chemical Reagent

Biochar (maple leaf) was obtained at this school. Additionally, the Tetracycline hydrochloride ( $\text{C}_{22}\text{H}_{25}\text{ClN}_2\text{O}_8$ ), potassium chloride (KCl), ascorbic acid (AA) and sodium acetate anhydrous ( $\text{CH}_3\text{COONa}$ ) were purchased from Chengdu Cologne Chemical Co., Ltd. (Chengdu, China). The potassium peroxymonosulfate ( $\text{KHSO}_5$ ), tert-butanol (TBA), humic acid ( $\text{C}_9\text{H}_8\text{Na}_2\text{O}_4$ ), methanol (MeOH), ferric chloride hexahydrate ( $\text{FeCl}_3 \cdot 6\text{H}_2\text{O}$ ), nitrate of potash ( $\text{KHNO}_3$ ) and sulfuric acid ( $\text{H}_2\text{SO}_4$ ) were obtained from Shanghai McLean Biochemical Technology Co., Ltd. (Shanghai, China). The disodium ethylenediaminetetraacetic acid (EDTA-2Na), sodium hydroxide (NaOH), potassium dihydrogen phosphate ( $\text{KH}_2\text{PO}_4$ ) and potassium bicarbonate ( $\text{KHCO}_3$ ) were provided by Guangzhou Jinhuada Chemical Reagent Co., Ltd. (Guangzhou, China). The absolute ethanol ( $\text{C}_2\text{H}_5\text{OH}$ ) was purchased from Chongqing Chuandong Chemical Co., Ltd. (Chongqing, China). The above reagents are analytical grade.

### 2.2. The Synthesize Method of $\text{FeO}_x\text{@BC}$

Specifically, the dried BC (maple leaf) was ground to a powder that could pass through a 100-mesh sieve. Secondly, 1.365 g ferric chloride hexahydrate ( $\text{FeCl}_3 \cdot 6\text{H}_2\text{O}$ ), 2.789 g sodium acetate anhydrous ( $\text{CH}_3\text{COONa}$ ) and the different mass ratio of BC was added to 5 mL anhydrous ethanol ( $\text{C}_2\text{H}_5\text{OH}$ ) and 2.5 mL deionized water, respectively. The obtained solid–liquid mixture was poured into a reaction still after stirring for 0.5 h, and reacted at 180 °C 12 h. After the hydrothermal carbonization reaction, the collected products were centrifuged and washed three times with anhydrous ethanol and water. Finally, the sample

is dried under vacuum at 50–60 °C for 8 h. The synthesis diagram of the FeO<sub>x</sub>@BC catalyst is presented in Figure 1.

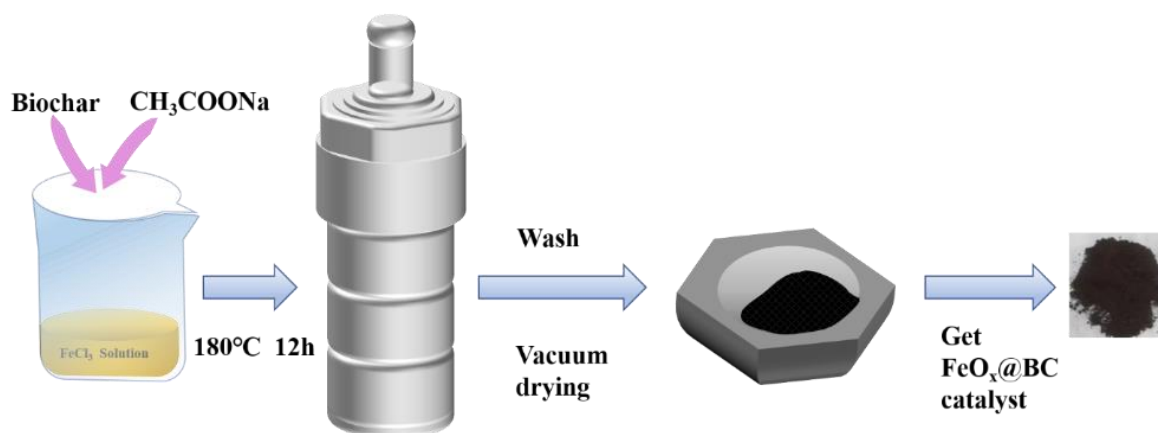


**Figure 1.** The synthesis diagram of FeO<sub>x</sub>@BC.

### 2.3. Characterization

The crystal structure and morphology of the catalyst were determined by XRD (Shimadzu, Japan), SEM (Carl Zeiss AG, Germany) and TEM/HRTEM (FEI Tecnai G2 f20 s-twin, USA). Additionally, the functional groups on the surface of the prepared catalyst were analyzed by FT-IR (Shimadzu, Japan). The porous textural parameters were obtained using a specific surface area and a pore-size analyzer (McASAP 2460/2020, USA). The band gap energy of the catalyst was measured by UV-vis (SHIMADU, Japan). The electron states of elements were analyzed by XPS (Thermo Fisher Scientific K-Alpha, Germany). SO<sub>4</sub><sup>2-</sup>•, •OH and O<sub>2</sub><sup>-</sup>• produced in the FeO<sub>x</sub>@BC + PMS + UVA-LED system were detected by EPR (JES-FA300, Japan).

### 2.4. Experimental Process

The experiment utilized a 500 mL glass beaker containing 300 mL of TC to be degraded. The magnetic stirrer was continuously stirred at 200 rpm and irradiated LED light (wavelength 405 nm).

Specifically, catalyst performance was investigated in the FeO<sub>x</sub>@BC + PMS + UVA-LED system on TC degradation efficiency. Firstly, different single process parameters experiments were investigated, including the mass ratio of Fe to BC, catalyst concentrations, PMS concentrations, initial concentrations of TC, reaction temperatures, and initial pHs. Since natural water contains inorganic anions and organic matter, the effect of coexisting anions (Cl<sup>-</sup>, HCO<sub>3</sub><sup>-</sup>, H<sub>2</sub>PO<sub>4</sub><sup>-</sup>, SO<sub>4</sub><sup>2-</sup>, NO<sub>3</sub><sup>-</sup>) and humic acid on TC degradation efficiency was discussed. Furthermore, the recycles performance was researched to discuss the reusable activity of the catalyst. Finally, the quenching experiments revealed possible reactive oxygen species (ROS).

The taken-out TC solution passed through a filter head with a pore size of 0.22 μm during TC degradation to obtain a transparent TC treatment solution. Then, the absorbance was measured by the spectrophotometer at 357 nm. Its efficiency is calculated in Equation (1), and the second-order k is shown in Equation (2).

$$\text{TC degradation rate} = (C_0 - C_t)/C_t \times 100\% \quad (1)$$

$$(1/C_t - 1/C_0) = kt \quad (2)$$

where k is the second-order reaction rate constant, C<sub>0</sub> is the initial TC concentration, and C<sub>t</sub> is the concentration of TC at a certain time t.

### 3. Results and Discussion

#### 3.1. Characterization

The crystal structure of  $\text{FeO}_x\text{@BC}$  catalyst was analyzed by XRD, as demonstrated in Figure 2a. The wide diffraction peaks from  $20^\circ$  to  $25^\circ$  correspond to C (002)—amorphous carbon [12]. Major diffraction peaks were detected at  $2\theta$  of  $30.09^\circ$ ,  $35.42^\circ$ ,  $43.05^\circ$ , and  $62.52^\circ$ , corresponding to the (220), (311), (400) and (440) crystal planes of magnetite (PDF#19-0629). The presence of Fe(III) and Fe(II) in the  $\text{FeO}_x\text{@BC}$  catalyst was subsequently proved.

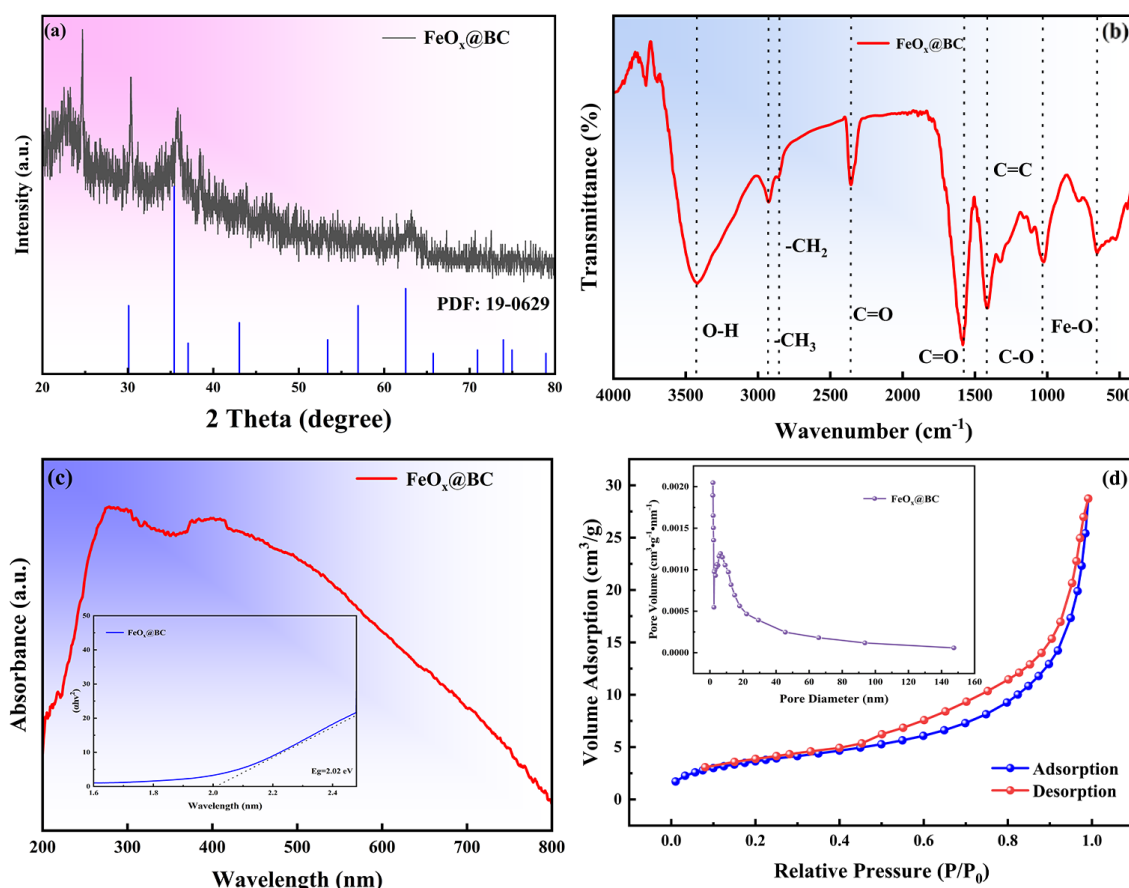


**Figure 2.** The  $\text{FeO}_x\text{@BC}$  catalyst XRD pattern (a), FT-IR spectra (b), UV-vis absorption spectra (c),  $\text{N}_2$  adsorption isotherms and pore size distribution curves (inset) (d).

Furthermore, the functional groups and structure of  $\text{FeO}_x\text{@BC}$  catalyst were analyzed by FT-IR spectra (Figure 2b). A peak was detected at  $3427\text{ cm}^{-1}$ , belonging to the O-H bond of water produced by hydrogen bonding on the  $\text{FeO}_x\text{@BC}$  catalyst [15]. And then the characteristic peaks of  $2931\text{ cm}^{-1}$  and  $2850\text{ cm}^{-1}$  were related to  $-\text{CH}_3$  and  $-\text{CH}_2$ , respectively [16]. The peaks of  $2358\text{ cm}^{-1}$  and  $1587\text{ cm}^{-1}$  both correspond to the C=O bond, but differ in that the former is attributable to  $\text{CO}_2$  in the air and the latter to tensile vibrations on the biochar [12,17]. As a supplement, the tensile vibrations of  $1421\text{ cm}^{-1}$  and  $1028\text{ cm}^{-1}$  were confirmed as C=C bonds and C-O bonds [18]. The tensile vibrations between  $800\text{ cm}^{-1}$  and  $500\text{ cm}^{-1}$  were associated with Fe-O bonds [19].

The optical properties of the  $\text{FeO}_x\text{@BC}$  catalyst were investigated via UV-vis absorption spectra with the results described in Figure 2c. The catalyst illustrates strong absorption of visible light, which means that the photoadsorption range is wide. With an  $E_g$  value of 2.02 eV, the narrow band gap can extremely enhance the utilization efficiency of visible light and promote the generation of photoinduced carriers with stronger photocatalytic activity [20].

Additionally, the specific surface area is also a key factor affecting the catalytic performance.  $\text{FeO}_x@BC$  was analyzed by BET,  $S_{\text{BET}}$ , pore volume and average pore size are shown in Table 1. The  $S_{\text{BET}}$  of  $\text{FeO}_x@BC$  is  $13.4921 \text{ m}^2/\text{g}$ , which has a large specific surface area to provide more active sites for the reaction. The adsorption–desorption curve of  $\text{FeO}_x@BC$  belongs to a type III isotherm and has an H4-type hysteresis loop, which means the irregular mesoporous structure is formed by aggregated particles [21]. Figure 2d (inset) shows that with the increase in pore size, the overall pore volume decreases, meaning, better surface properties of  $\text{FeO}_x@BC$ .

**Table 1.** The BET surface areas, pore volumes and average pore diameter of  $\text{FeO}_x@BC$  catalyst.

Samples	$S_{\text{BET}}$ ( $\text{m}^2/\text{g}$ )	Pore Volume ( $\text{cm}^3/\text{g}$ )	Average Pore Diameter (nm)
$\text{FeO}_x@BC$	13.4921	0.0441	13.9219

The surface morphologies of the  $\text{FeO}_x@BC$  catalyst at different magnifications were observed, as plotted in Figure 3. It is granular and well-dispersed, and the surface is relatively smooth with a size of 100 nm–200 nm. Figure 3d shows the mapping images of the  $\text{FeO}_x@BC$  catalyst, in which three presented elements, C, Fe, and O, are uniformly dispersed.

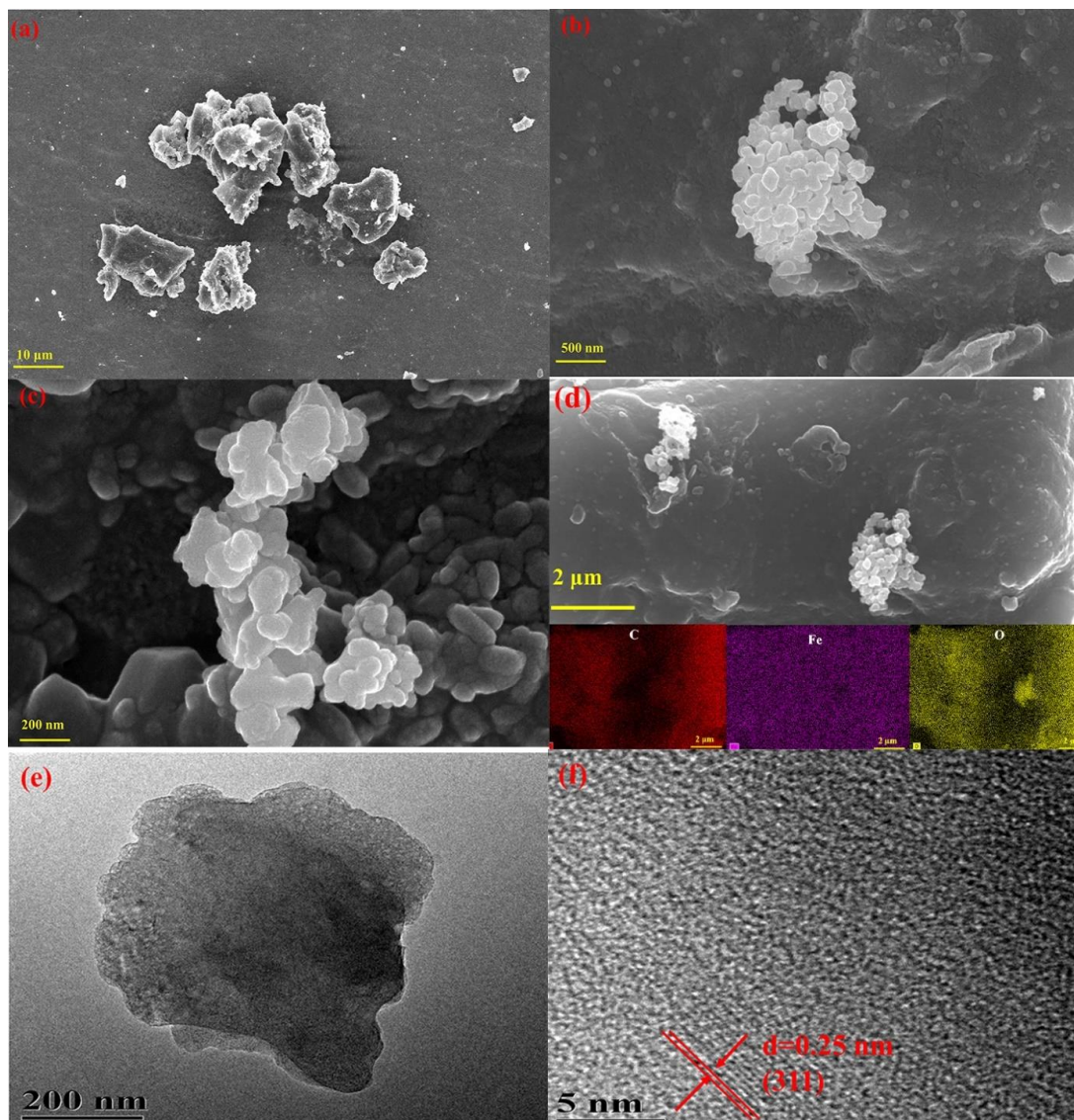


**Figure 3.** SEM images (a–c) and mapping images (d) of  $\text{FeO}_x@BC$ , TEM/HRTEM images (e,f).

The morphology of the catalyst was further analyzed by TEM/HRTEM, as presented in Figure 3e, f. The lattice fringe spacing of 0.25 nm corresponds to the (311) crystal plane of magnetite, indicating that this plane is the dominantly exposed crystal plane.

### 3.2. TC Removal in Different Treatment Systems

The corresponding control experiments were investigated, as presented in Figure 4. The degradation efficiency of TC basically did not degrade with only  $\text{FeO}_x$ @BC catalyst, which suggested that the adsorption ability of the catalyst was finite. Additionally, its efficiency was not enhanced in the  $\text{FeO}_x$ @BC + UVA-LED system. It was proved that the catalyst cannot be photodegraded and must be activated by oxidants. The efficiency was slightly enhanced by adding PMS, but it was still relatively low. Results confirmed that the oxidation capacity of PMS was weak without other activation methods. Subsequently, its efficiency did not raise after adding  $\alpha\text{-Fe}_2\text{O}_3$ , which evidenced that Fe(III) did not activate PMS. Ultimately, the UVA-LED irradiation significantly improved its efficiency compared with the  $\text{FeO}_x$ @BC + PMS system. This situation can be explained that the dramatic improvement of Fe(II)/Fe(III) conversion capacity under the synergistic effect of visible light and PMS, thus continuously activating PMS to degrade TC.

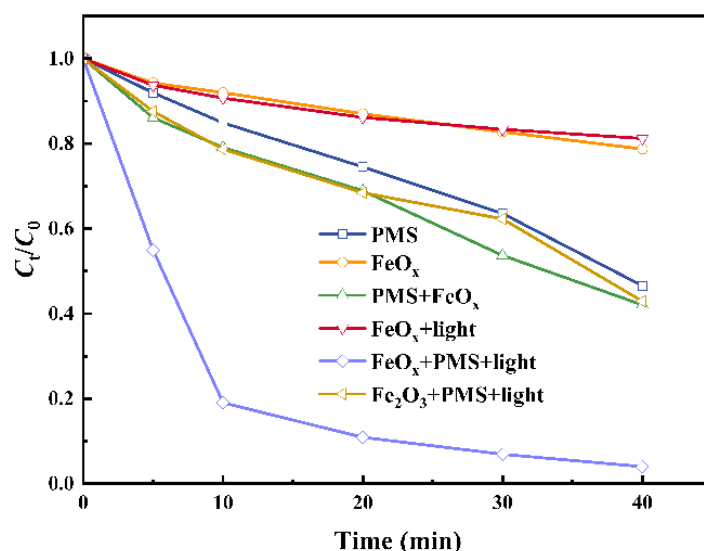


**Figure 4.** Control experiment. (Reaction conditions: catalyst concentration = 0.2 g/L, PMS concentration = 3 mM, TC initial concentration = 40 mg/L, reaction temperature = 25 °C, initial pH = 5.5).

### 3.3. Effect of Process Parameters on TC Degradation

In general, the performance of the catalyst varies with the composition of the element. Figure 5a depicted the degradation efficiency of TC, in which  $\text{FeO}_x$ @BC in different proportions activated PMS under UVA-LED irradiation. Its efficiency was the highest with the mass ratio of Fe to BC being 1:3, which can be explained that the Fe(II) content in the catalyst also increased with the increase of BC, and then activating the PMS to produce more ROS. On the other hand, it can be explained that  $\text{FeO}_x$  can improve the carrier utilization efficiency by easily accepting the photoexcited electrons of BC, thus ensuring that a considerable number of photogenerated holes are left on  $\text{FeO}_x$  to participate in the degradation of TC [22]. However, its efficiency of TC, inhibited as BC, was increasing further because more BC inhibits the activity of the  $\text{FeO}_x$  catalyst. In summary,  $\text{FeO}_x$ @BC catalysts with a mass ratio of Fe to BC of 1:3 were selected for further experiments.

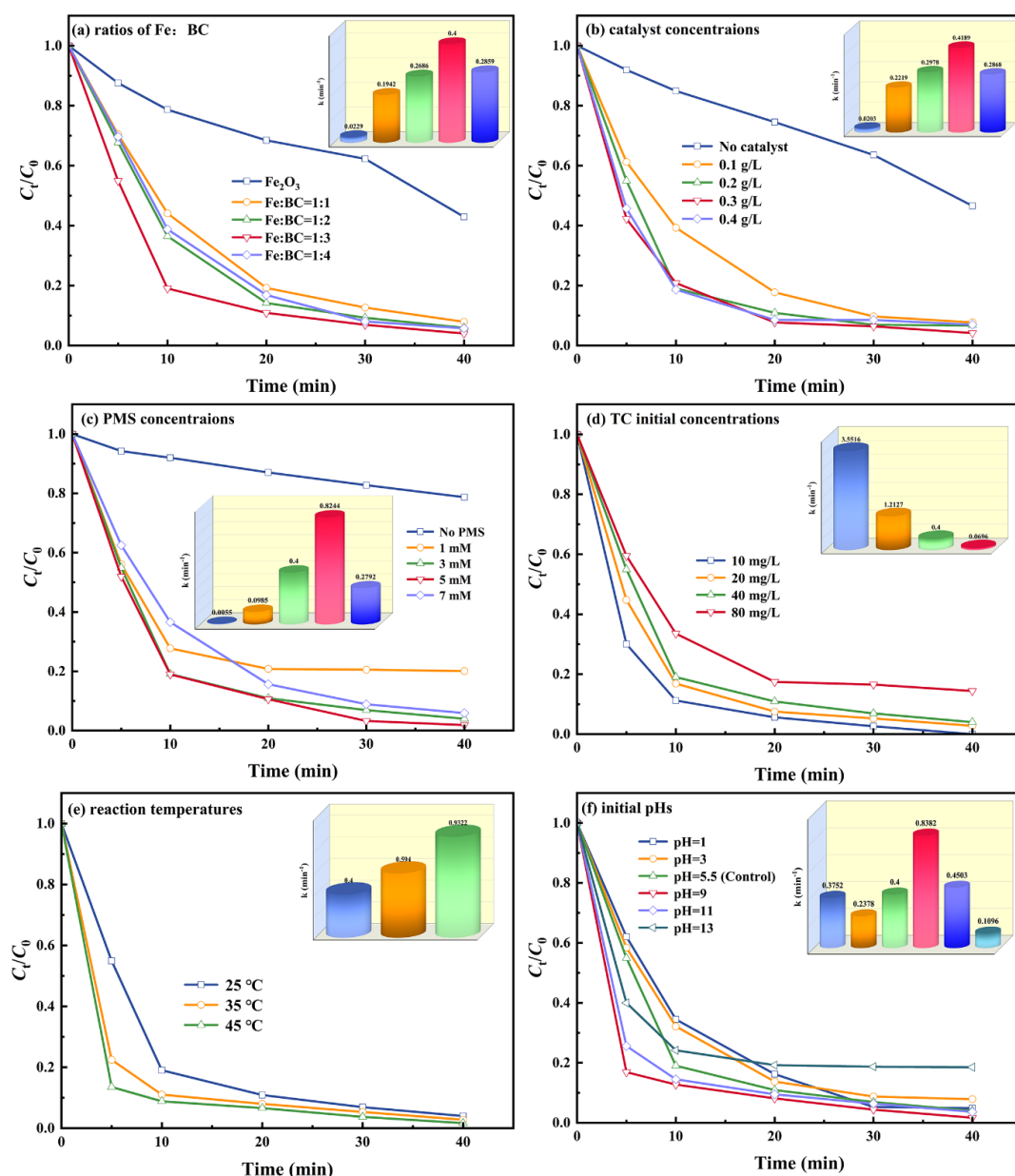


**Figure 5.** The effect of (a) the mass ratio of Fe:BC, (b) catalyst concentrations, (c) PMS concentrations, (d) initial concentrations of TC, (e) reaction temperatures, (f) initial pHs on the degradation of TC in the  $\text{FeO}_x\text{@BC}$  + PMS + UVA-LED system, and the inset is the reaction rate constant  $k$ .

The catalyst plays a dramatic role in providing active sites for PMS, and its concentration directly affects the efficiency. As presented in Figure 5b, first, the efficiency gradually enhanced and then stabilized. This situation was because more active sites were provided for PMS, thus more ROS were generated to degrade TC. Additionally, the reason for the stabilization may be that the excess catalyst cannot provide more ROS without additional PMS activation. However, catalyst waste can occur.

The PMS concentration is a major factor affecting the degradation of organic pollutants in wastewater. Hence, different concentrations of PMS on TC degradation efficiency were investigated (Figure 5c). It was only 21% in 40 min in the absence of  $\text{FeO}_x\text{@BC}$  catalyst. A possible reason for this phenomenon could be that the adsorption capacity of the catalyst was limited. Moreover, its efficiency was significantly strengthened with the concentration of PMS, increasing from 1 mM to 5 mM. This was because PMS was prompted to contact with the catalyst, and generated ROS. However, its efficiency tended to decline with the

concentration of PMS increasing further, because excessive PMS quenched  $\text{SO}_4^{\cdot-}$ , as plotted in Equations (3) and (4) [23].



Figure 5d elucidated the changing trend of TC initial concentration from 10 mg/L to 80 mg/L, and its efficiency gradually decreased. It can be explained by the constant concentration of catalyst and PMS, while the increase of TC molecules required more ROS, resulting in the decline of its efficiency.

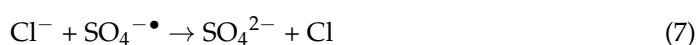
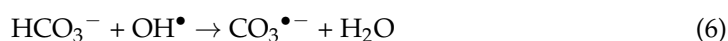
Three different temperature gradients were set up to explore whether the temperature had an effect on TC degradation efficiency (Figure 5e). Its degradation efficiency of TC at 45 °C was much higher than that at 35 °C and 25 °C. This was due to temperature rise being beneficial for the degradation of TC, and also provided evidence that the system was an endothermic reaction. Moreover, increasing the temperature encouraged the formation of more ROS between the PMS and the catalyst [24]. However, higher temperatures mean higher energy input, so the cost in practical applications was considered.

pH may affect the surface electrical properties of the catalyst, and the dissociation state of the target compound from the PMS [25]. As demonstrated in Figure 5f, TC degradation was inhibited under acidic conditions, because  $\text{H}^+$  was more likely to form hydrogen bonds with O-O of  $\text{HSO}_5^-$ , and it was difficult to produce  $\text{SO}_4^{\cdot-}$  [26]. Moreover, the degradation of TC was highest under weak alkaline conditions (pH = 9). This can be explained as the weakly alkaline conditions were conducive to protecting the surface crystallinity of the catalyst, and it can effectively prevent metal from leaching into the reaction solution, thus inducing the formation of more  $\text{HSO}_5^-$  to generate  $\text{SO}_4^{\cdot-}$ . On the other hand, the pH under weak alkaline conditions was more conducive to the formation of  $\cdot\text{OH}$ . However, the electrostatic repulsion between the strong alkaline PMS and the catalyst surface inhibited the catalytic activity, resulting in the hindrance of the TC's degradation efficiency.

### 3.4. Effect of Coexisting Anions and Humic Acid

Various anions and humic acid exist widely in real water, which may affect the production of ROS in the degradation reaction, and then affect efficiency. Therefore, various anions ( $\text{H}_2\text{PO}_4^-$ ,  $\text{NO}_3^-$ ,  $\text{HCO}_3^-$ ,  $\text{Cl}^-$ ,  $\text{SO}_4^{2-}$ ) were added separately to the  $\text{FeO}_x\text{@BC}$  + PMS + UVA-LED system to investigate their influences (Figure 6a). In general, TC degradation efficiency was inhibited to varying degrees by these anions. Notably,  $\text{H}_2\text{PO}_4^-$  had the strongest effect on inhibiting TC because it presented a strong adsorption capacity on the catalyst surface, and formed a complex within iron ions to block the active site [27]. Secondly, TC degradation was hindered by  $\text{HCO}_3^-$ , explained via the fact that  $\text{HCO}_3^-$  would consume ROS generated in the reaction and generate  $\text{CO}_3^{\cdot-}$ , as shown in Equations (5) and (6) [28]. Furthermore,  $\text{Cl}^-$  and  $\text{SO}_4^{2-}$  had a slight inhibitory effect on TC degradation due to their reaction with  $\text{SO}_4^{\cdot-}$ , as shown in Equations (7)–(11) [28,29].

Humic acid (HA) widely exists in real surface water and is the main organic pollutant in the wastewater process. Figure 6b illustrated the effect of HA on TC degradation efficiency in the  $\text{FeO}_x\text{@BC}$  + PMS + UVA-LED system. The efficiency was still as high as 85.2% within 40 min at a low concentration of HA (30 mg/L). While its efficiency showed a strong inhibitory effect with HA increasing by 60 mg/L, which was due to the adsorption of phenolic hydroxyl and carboxyl groups of HA at the catalyst site, thus exposing less active sites to contact with PMS [30].



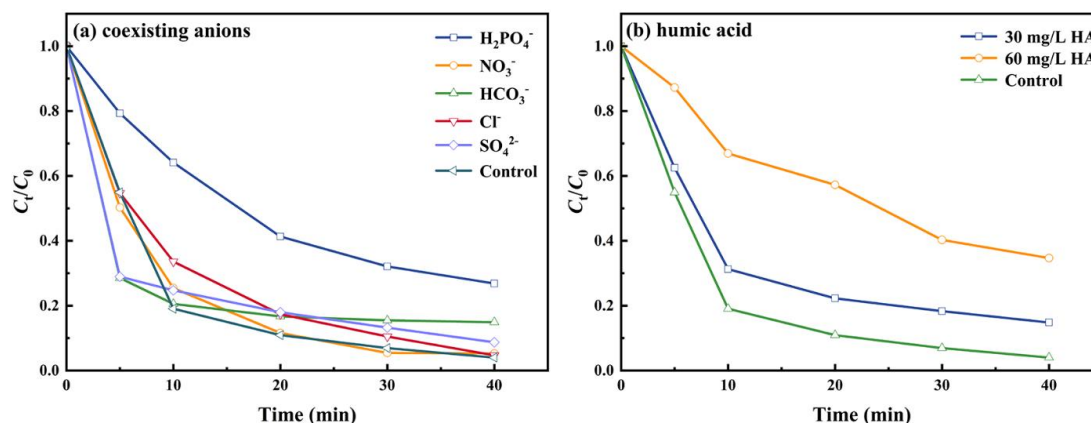
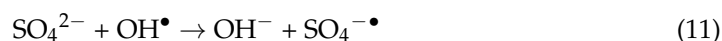
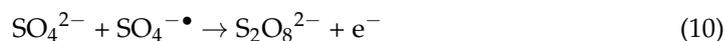


**Figure 6.** The effect of (a) coexisting anions, (b) humic acid on the degradation of TC in the  $\text{FeO}_x\text{@BC}$  + PMS + UVA-LED system.

### 3.5. Reusable Performance of $\text{FeO}_x\text{@BC}$ Catalyst

The reusable performance of catalysts is important in practical applications. Consequently, it activated PMS on TC degradation under UVA-LED irradiation in five cycles that were researched (Figure 7a). The efficiency of the second to fifth reuses was marginal, because the adsorption of TC byproducts on the surface of the catalyst resulted in a small part of the active site being blocked. But its degradation efficiency was still as high as 80%. Furthermore, the structural stability of the catalyst was researched by FT-IR spectra. FT-IR spectra analysis, after repeated use five times, presents no change compared with fresh FT-IR spectra (Figure 7b). The results evidenced that the catalyst had excellent catalytic, stability and reusable performance. The system is compared with the previously reported  $\text{FeO}_x$ -doped BC catalyst, as demonstrated in Table 2. Finally, it is confirmed that the  $\text{FeO}_x\text{@BC}$ -activated PMS has the highest degradation efficiency and excellent cycling performance.

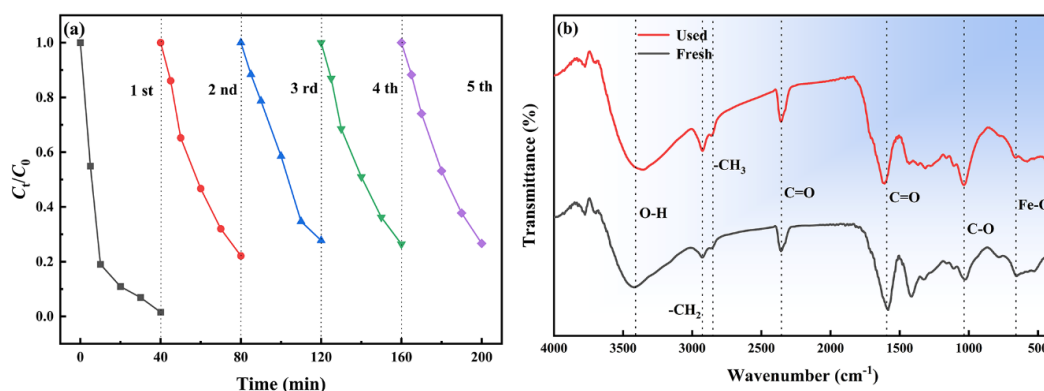


**Figure 7.** The reusability of catalyst activated PMS for TC degradation (a), FT-IR spectra before and after TC degradation by  $\text{FeO}_x\text{@BC}$ . (Reaction conditions: catalyst concentration = 0.2 g/L, PMS concentration = 3 mM, TC initial concentration = 40 mg/L, reaction temperature = 25 °C, initial pH = 5.5).

**Table 2.** Comparison of TC degradation performance of the FeO<sub>x</sub> catalyst-doped BC-activated PMS.

Catalyst Type	TC Initial Concentration	Other Experimental Conditions	Degradation Efficiency	Reusability Performance (Reuse Times, Residual Degradation Efficiency)	Reference
CoFe <sub>2</sub> O <sub>4</sub> /BC	20 mg/L	Catalyst dosage = 0.5 g/L, PMS concentration = 0.977 mM, Temperature = 25 °C, Initial pH = 5.5	99.8% (30 min)	5 times, 96.39%	[31]
Fe-Mn/AW-BC	20 mg/L	Catalyst dosage = 0.5 g/L, PMS concentration = 0.5 mM, Temperature = 30 °C, Initial pH = 4.79	97.9% (60 min)	5 times, 77.8%	[32]
Co-Fe@PPBC	50 mg/L	Catalyst dosage = 0.1 g/L, PMS concentration = 1 g/L,	86.91% (60 min)	5 times, 61.14%	[33]
FeO <sub>x</sub> @BC	40 mg/L	Catalyst dosage = 0.2 g/L, PMS concentration = 3 mM, Temperature = 25 °C, Initial pH = 5.5,	96% (40 min)	5 times, 80%	This study

### 3.6. Reaction Mechanism and Possible ROS

To explore the ROS formed in the FeO<sub>x</sub>@BC + PMS + UVA-LED system through quenching experiments, tert-Butanol (TBA) was used to quench •OH, while methanol (MeOH) is a quencher of •OH and SO<sub>4</sub><sup>•-</sup>, so •OH and SO<sub>4</sub><sup>•-</sup> can be distinguished by it [34]. As shown in Figure 8a, 0.3 mol/L TBA produced a slight inhibition effect on TC degradation, while the inhibition effect was significantly enhanced with the concentration increased to 0.6 mol/L because improving the TBA concentration could quench more •OH in the reaction system. Moreover, it is shown that the inhibition effect of MeOH was always stronger than that of TBA (MeOH would have a mask effect on the FeO<sub>x</sub>@BC catalyst surface), which also evidenced that SO<sub>4</sub><sup>•-</sup> contributed to the reaction process of TC degradation. Additionally, EDTA disodium salt (EDTA-2Na) was selected as the scavenger for the hole effect (h<sup>+</sup>) [35]. As presented in Figure 8b, the inhibition of EDTA-2Na on TC degradation was extremely obvious because EDTA-2Na hindered the reaction between hole and water molecule produces •OH [36]. Additionally, ascorbic acid (AA) is considered to be a quencher of superoxide free radicals (O<sub>2</sub><sup>•-</sup>). The degradation of TC was hindered by AA of different concentrations, and the inhibitory effect became increasingly more obvious with concentration enhancement.

The corresponding EPR test was performed with DMPO to better determine the role of ROS in the FeO<sub>x</sub>@BC + PMS + UVA-LED system. As manifested in Figure 8c, the signals of SO<sub>4</sub><sup>•-</sup> and •OH for 0 min, 2 min, 5 min and 10 min were determined, respectively. It is shown that SO<sub>4</sub><sup>•-</sup> and •OH were generated during the degradation reaction, and their signal intensity became stronger with the increase of time. It furtherly confirmed the ability of FeO<sub>x</sub>@BC to activate PMS and was also consistent with the results of the quenching experiment in Figure 8a. Moreover, O<sub>2</sub><sup>•-</sup> strongly signals were detected in the FeO<sub>x</sub>@BC + PMS + UVA-LED system (Figure 8d). A possible reason for the phenomenon was that O<sub>2</sub><sup>•-</sup> was produced by the electron transfer of O<sub>2</sub>. Furthermore, O<sub>2</sub><sup>•-</sup> contributed to the cycle of Fe(III) to Fe(II), and also contributed to the activation of PMS to produce SO<sub>4</sub><sup>•-</sup> [37].

To reveal the reaction mechanism in the FeO<sub>x</sub>@BC + PMS + UVA-LED system, the FeO<sub>x</sub>@BC catalyst was investigated by XPS spectra. As elucidated in Figure 9a, the spectra of XPS did not change significantly before and after the reaction, so it was necessary to further investigate the high-resolution XPS spectra of C, Fe and O.

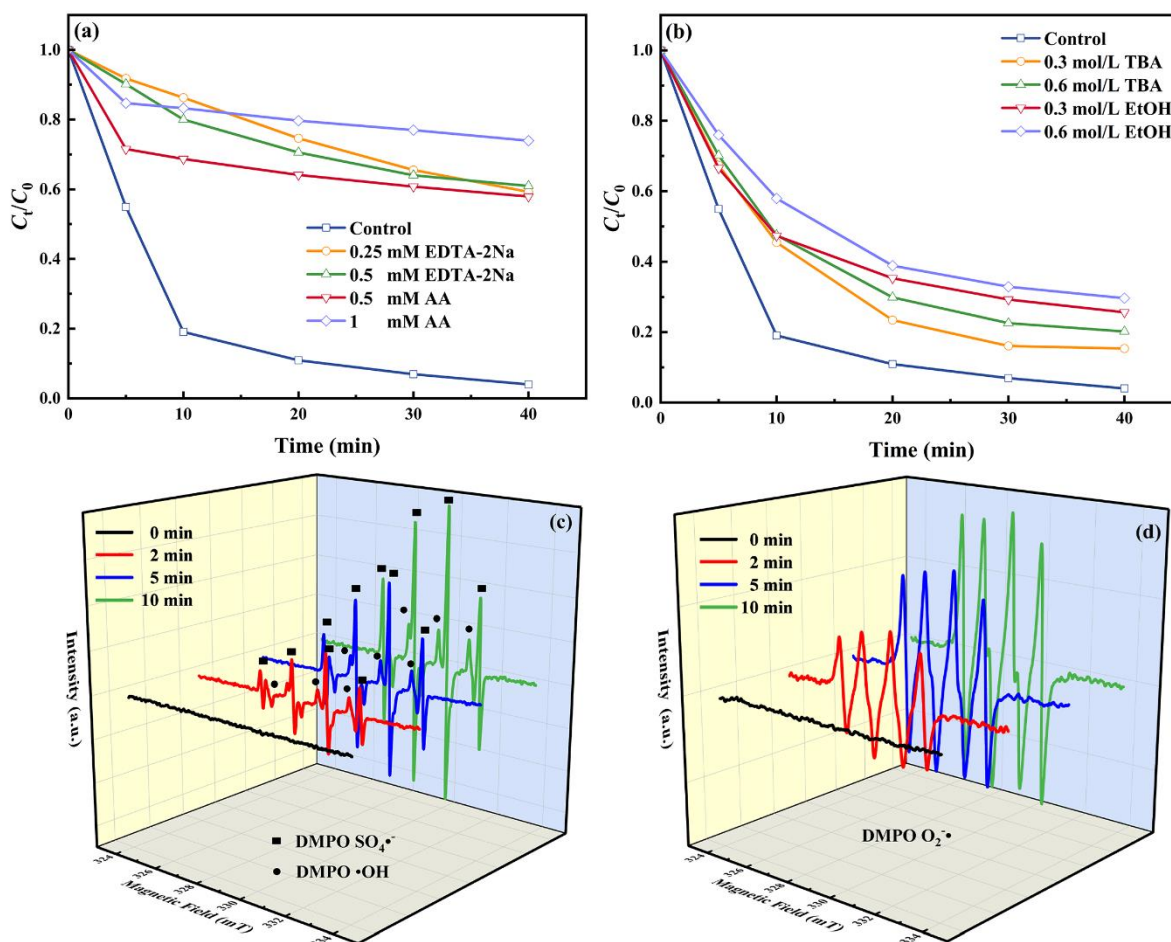


Figure 8. Effect of ROS quenchers on TC degradation (a,b); EPR tests of  $\text{SO}_4^{\bullet-}$  and  $\bullet\text{OH}$  (c) and  $\text{O}_2^{\bullet-}$  (d).

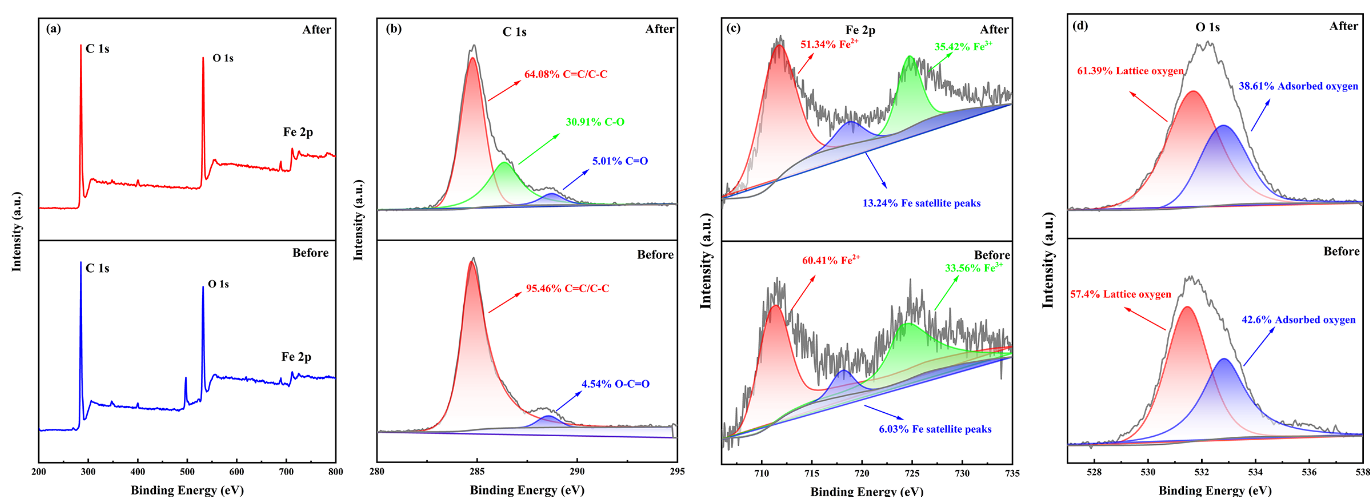


Figure 9. XPS spectra of  $\text{FeO}_x@BC$  catalyst before and after reaction (a), C 1s (b), Fe 2p (c), O 1s (d).

The spectra of C 1s before and after the reaction were illustrated in Figure 9b, which can be fitted into two peaks at 284.69 eV and 288.55 eV, associated with the C-C/C=C bond and O-C=O bond, respectively [38]. Additionally, C-C/C=C, C-O, C=O [39] was fitted for the three peaks, respectively, after the degradation reaction in 284.77 eV and 286.35 eV and 288.72 eV. Evidentially, the contents of C-C/C=C and O-C=O bonds changed slightly, which showed that the catalyst had stability in long-term use.



#### 4. Conclusions

In summary, the FeO<sub>x</sub>@BC catalyst was prepared by the hydrothermal method using waste maple leaf as a carbon source and FeCl<sub>3</sub>•6H<sub>2</sub>O as an iron source. Due to the synergistic effect of UVA-LED irradiation and PMS, the degradation efficiency of TC reached 96% within 40 min. Notably, FeO<sub>x</sub>@BC maintained excellent efficiency and performance in regeneration experiments, and the degradation efficiency was still as high as 80% after five cycles. The active free radicals involved in TC degradation were SO<sub>4</sub><sup>•-</sup>, •OH, O<sub>2</sub><sup>•-</sup> and h<sup>+</sup> by quenching experiments and EPR tests. This study provides a feasible idea for FeO<sub>x</sub> catalyst-doped BC to activate PMS to degrade TC wastewater.

**Author Contributions:** P.C.: Methodology, Formal analysis, Investigation, Data curation, Writing—Original draft. L.Z.: Software, Investigation. Z.C.: Conceptualization; Supervision; Writing—original draft; Review and editing; Funding acquisition. J.T.: Resources. H.H.: Methodology, Investigation. C.J.: Original draft, Software. Z.W.: Methodology, Writing—review and editing, Supervision. All authors have read and agreed to the published version of the manuscript.

**Funding:** This research was sponsored by the Special Key Program of Technological Innovation and Application Development of Chongqing (CSTB2022TIADKPX0128), the Youth Project of Science and Technology Research Program of Chongqing Education Commission of China (KJQN202001148), the Natural Science Foundation of Chongqing, China (cstc2020jcyj-msxmX0308), and Research Program from Chongqing Water Group Co., LTD (2023Q295). Here we sincerely thank all the sponsors.

**Data Availability Statement:** The data presented in this study are available on request from the authors.

**Conflicts of Interest:** The authors declare no conflict of interest.

#### References

1. Yan, C.; Cheng, Z.; Wei, J.; Xu, Q.; Zhang, X.; Wei, Z. Efficient degradation of antibiotics by photo-Fenton reactive ceramic membrane with high flux by a facile spraying method under visible LED light. *J. Clean. Prod.* **2022**, *366*, 132849. [[CrossRef](#)]
2. Zhang, Z.; Wang, Z.; Tan, J.; Zhou, K.; Garcia-Meza, J.V.; Song, S.; Xia, L. Yeast-derived biochar to load CoFe<sub>2</sub>O<sub>4</sub>: Degradation of tetracycline hydrochloride by heterogeneous activation of peroxymonosulfate. *J. Environ. Chem. Eng.* **2023**, *11*, 110020. [[CrossRef](#)]
3. Alok, A.; Chaudhury, N.K. Tetracycline hydrochloride: A potential clinical drug for radioprotection. *Chem. Biol. Interact.* **2016**, *245*, 90–99. [[CrossRef](#)]
4. Li, X.; Liu, C.; Chen, Y.; Huang, H.; Ren, T. Antibiotic residues in liquid manure from swine feedlot and their effects on nearby groundwater in regions of North China. *Environ. Sci. Pollut. Res.* **2018**, *25*, 11565–11575. [[CrossRef](#)] [[PubMed](#)]
5. Chen, F.; Wu, X.L.; Yang, L.; Chen, C.; Lin, H.; Chen, J. Efficient degradation and mineralization of antibiotics via heterogeneous activation of peroxymonosulfate by using graphene supported single-atom Cu catalyst. *Chem. Eng. J.* **2020**, *394*, 124904. [[CrossRef](#)]
6. Ji, F.; Zhang, H.; Wei, X.; Zhang, Y.; Lai, B. Efficient degradation of atrazine by Co-NZ catalyst prepared by electroless plating in the presence of peroxymonosulfate: Characterization, performance and mechanistic consideration. *Chem. Eng. J.* **2019**, *359*, 1316–1326. [[CrossRef](#)]
7. Phan, H.T.B.; Nguyen, A.Q.K.; Ahn, Y.-Y.; Kim, K.; Kim, S.; Kim, J. Visible light-induced degradation of propranolol with peroxymonosulfate as an oxidant and a radical precursor. *Sep. Purif. Technol.* **2022**, *289*, 120764. [[CrossRef](#)]
8. Cai, H.; Zou, J.; Lin, J.; Li, J.; Huang, Y.; Zhang, S.; Yuan, B.; Ma, J. Sodium hydroxide-enhanced acetaminophen elimination in heat/peroxymonosulfate system: Production of singlet oxygen and hydroxyl radical. *Chem. Eng. J.* **2022**, *429*, 132438. [[CrossRef](#)]
9. Ghanbari, F.; Moradi, M. Application of peroxymonosulfate and its activation methods for degradation of environmental organic pollutants: Review. *Chem. Eng. J.* **2016**, *310*, 307–315. [[CrossRef](#)]
10. Qi, C.; Liu, X.; Lin, C.; Zhang, X.; Ma, J.; Tan, H.; Ye, W. Degradation of sulfamethoxazole by microwave-activated persulfate: Kinetics, mechanism and acute toxicity. *Chem. Eng. J.* **2014**, *249*, 6–14. [[CrossRef](#)]
11. Chen, Y.-A.; Wang, Y.-T.; Moon, H.S.; Yong, K.; Hsu, Y.-J. Yolk-shell nanostructures: Synthesis, photocatalysis and interfacial charge dynamics. *RSC Adv.* **2021**, *11*, 12288–12305. [[CrossRef](#)] [[PubMed](#)]
12. Wang, M.; Wang, Y.; Li, Y.; Wang, C.; Kuang, S.; Ren, P.; Xie, B. Persulfate oxidation of tetracycline, antibiotic resistant bacteria, and resistance genes activated by Fe doped biochar catalysts: Synergy of radical and non-radical processes. *Chem. Eng. J.* **2023**, *464*, 142558. [[CrossRef](#)]
13. Ye, Q.; Wu, J.; Wu, P.; Rehman, S.; Ahmed, Z.; Zhu, N. Enhancing peroxymonosulfate activation by Co-Fe layered double hydroxide catalysts via compositing with biochar. *Chem. Eng. J.* **2021**, *417*, 129111. [[CrossRef](#)]
14. Tao, S.; Liang, S.; Chen, Y.; Yu, W.; Qiu, J.; Zhu, Y.; Xiao, K.; Hu, J.; Liu, B.; Wang, Y.; et al. Enhanced sludge dewaterability with sludge-derived biochar activating hydrogen peroxide: Synergism of Fe and Al elements in biochar. *Water Res.* **2020**, *182*, 115927. [[CrossRef](#)] [[PubMed](#)]

15. Xi, M.; Cui, K.; Cui, M.; Ding, Y.; Guo, Z.; Chen, Y.; Li, C.; Li, X. Enhanced norfloxacin degradation by iron and nitrogen co-doped biochar: Revealing the radical and nonradical co-dominant mechanism of persulfate activation. *Chem. Eng. J.* **2021**, *420*, 129902. [[CrossRef](#)]
16. He, J.; Xiao, Y.; Tang, J.; Chen, H.; Sun, H. Persulfate activation with sawdust biochar in aqueous solution by enhanced electron donor-transfer effect. *Sci. Total Environ.* **2019**, *690*, 768–777. [[CrossRef](#)]
17. Zhang, Y.; Chen, M.; Zhang, Z.; Jiang, Z.; Shangguan, W.; Einaga, H. Simultaneously catalytic decomposition of formaldehyde and ozone over manganese cerium oxides at room temperature: Promotional effect of relative humidity on the MnCeO<sub>x</sub> solid solution. *Catal. Today* **2019**, *327*, 323–333. [[CrossRef](#)]
18. Zhu, K.; Shen, Q.; Huang, Y.; He, J.; Chen, D.; Wen, J. In-situ formed N-doped bamboo-like carbon nanotubes encapsulated with Fe nanoparticles supported by biochar as highly efficient catalyst for activation of persulfate (PS) toward degradation of organic pollutants. *Chem. Eng. J.* **2020**, *402*, 126090. [[CrossRef](#)]
19. Zhu, S.; Wang, Z.; Ye, C.; Deng, J.; Ma, X.; Xu, Y.; Wang, L.; Tang, Z.; Luo, H.; Li, X. Magnetic Co/Fe nanocomposites derived from ferric sludge as an efficient peroxymonosulfate catalyst for ciprofloxacin degradation. *Chem. Eng. J.* **2022**, *432*, 134180. [[CrossRef](#)]
20. Chen, H.; Zhang, X.; Jiang, L.; Yuan, X.; Liang, J.; Zhang, J.; Yu, H.; Chu, W.; Wu, Z.; Li, H. Strategic combination of nitrogen-doped carbon quantum dots and g-C<sub>3</sub>N<sub>4</sub>: Efficient photocatalytic peroxydisulfate for the degradation of tetracycline hydrochloride and mechanism insight. *Sep. Purif. Technol.* **2021**, *272*, 118947. [[CrossRef](#)]
21. Liu, Y.; Liu, X.; Zhao, Y.; Dionysiou, D.D. Aligned  $\alpha$ -FeOOH nanorods anchored on a graphene oxide-carbon nanotubes aerogel can serve as an effective Fenton-like oxidation catalyst. *Appl. Catal. B* **2017**, *213*, 74–86. [[CrossRef](#)]
22. Lin, Y.-F.; Hsu, Y.-J. Interfacial charge carrier dynamics of type-II semiconductor nanoheterostructures. *Appl. Catal. B* **2013**, *130–131*, 93–98. [[CrossRef](#)]
23. Hussain, I.; Li, M.; Zhang, Y.; Li, Y.; Huang, S.; Du, X.; Liu, G.; Hayat, W.; Anwar, N. Insights into the mechanism of persulfate activation with nZVI/BC nanocomposite for the degradation of nonylphenol. *Chem. Eng. J.* **2017**, *311*, 163–172. [[CrossRef](#)]
24. Shuchi, S.B.; Suhan, M.B.K.; Humayun, S.B.; Haque, M.E.; Islam, M.S. Heat-activated potassium persulfate treatment of Sudan Black B dye: Degradation kinetic and thermodynamic studies. *J. Water Process. Eng.* **2020**, *39*, 101690. [[CrossRef](#)]
25. Ma, Y.; Wang, D.; Xu, Y.; Lin, H.; Zhang, H. Nonradical electron transfer-based peroxydisulfate activation by a Mn-Fe bimetallic oxide derived from spent alkaline battery for the oxidation of bisphenol A. *J. Hazard Mater.* **2022**, *436*, 129172. [[CrossRef](#)]
26. Zhu, L.; Shi, Z.; Deng, L.; Duan, Y. Efficient degradation of sulfadiazine using magnetically recoverable MnFe<sub>2</sub>O<sub>4</sub>/ $\delta$ -MnO<sub>2</sub> hybrid as a heterogeneous catalyst of peroxymonosulfate. *Colloids Surf. A Physicochem. Eng. Asp.* **2020**, *609*, 125637. [[CrossRef](#)]
27. Duan, P.; Ma, T.; Yue, Y.; Li, Y.; Zhang, X.; Shang, Y.; Gao, B.; Zhang, Q.; Yue, Q.; Xu, X. Fe/Mn nanoparticles encapsulated in nitrogen-doped carbon nanotubes as a peroxymonosulfate activator for acetamiprid degradation. *Environ. Sci. Nano* **2019**, *6*, 1799–1811. [[CrossRef](#)]
28. Boucheloukh, H.; Sehili, T.; Kouachi, N.; Djebbar, K. Kinetic and analytical study of the photo-induced degradation of monuron by nitrates and nitrites under irradiation or in the dark. *Photochem. Photobiol. Sci.* **2012**, *11*, 1339–1345. [[CrossRef](#)]
29. Jin, H.; Cang, Z.; Ding, W.; Wu, W.; Zhang, L. Oxidative removal of antibiotic resistant E. coli by sulfidated zero-valent iron: Homogeneous vs heterogeneous activation. *J. Hazard Mater.* **2020**, *408*, 124411. [[CrossRef](#)]
30. Li, M.; Li, Y.W.; Yu, P.F.; Zhao, H.M.; Xiang, L.; Feng, N.-X.; Li, Q.-K.; He, K.-Y.; Luo, X.; Cai, Q.-Y.; et al. Exploring degradation mechanism of tetracycline via high-effective peroxymonosulfate catalysts of montmorillonite hybridized CoFe composites and safety assessment. *Chem. Eng. J.* **2021**, *427*, 130930. [[CrossRef](#)]
31. Huang, N.; Wang, T.; Wu, Y.; Wang, F.; Zhang, D.; Zhou, R.; Kong, C.; Yang, Z.; Zhang, H.; Zhu, H. Preparation of magnetically recyclable hierarchical porous sludge-pine needle derived biochar loaded CoFe<sub>2</sub>O<sub>4</sub> nanoparticles for rapid degradation of tetracycline by activated PMS. *Mater. Today Commun.* **2023**, *35*, 106313. [[CrossRef](#)]
32. Liang, F.; Liu, Z.; Jiang, X.; Li, J.; Xiao, K.; Xu, W.; Chen, X.; Liang, J.; Lin, Z.; Li, M.; et al. NaOH-modified biochar supported Fe/Mn bimetallic composites as efficient peroxymonosulfate activator for enhance tetracycline removal. *Chem. Eng. J.* **2023**, *454*, 139949. [[CrossRef](#)]
33. Han, S.; Xiao, P. Catalytic degradation of tetracycline using peroxymonosulfate activated by cobalt and iron co-loaded pomelo peel biochar nanocomposite: Characterization, performance and reaction mechanism. *Sep. Purif. Technol.* **2022**, *287*, 120533. [[CrossRef](#)]
34. Xu, S.; Wen, L.; Yu, C.; Li, S.; Tang, J. Activation of peroxymonosulfate by MnFe<sub>2</sub>O<sub>4</sub>@BC composite for bisphenol A Degradation: The coexisting of free-radical and non-radical pathways. *Chem. Eng. J.* **2022**, *442*, 136250. [[CrossRef](#)]
35. Chen, N.; Lee, D.; Kang, H.; Cha, D.; Lee, J.; Lee, C. Catalytic Persulfate Activation for Oxidation of Organic Pollutants: A Critical Review on Mechanisms and Controversies. *J. Environ. Chem. Eng.* **2022**, *10*, 107654. [[CrossRef](#)]
36. Zheng, M.; Xing, C.; Zhang, W.; Cheng, Z.; Zhang, S. Hydrogenated hematite nanoplates for enhanced photocatalytic and photo-Fenton oxidation of organic compounds. *Inorg. Chem. Commun.* **2020**, *119*, 108040. [[CrossRef](#)]
37. Dat, O.; Chen, Y.; Yan, J.; Qian, L.; Lu, H.; Chen, M. Activation mechanism of peroxymonosulfate by biochar for catalytic degradation of 1,4-dioxane: Important role of biochar defect structures. *Chem. Eng. J.* **2019**, *370*, 614–624. [[CrossRef](#)]
38. Yang, J.; Li, P.; Wang, L.; Guo, X.; Liu, S. In-situ synthesis of Ni-MOF@CNT on graphene/Ni foam substrate as a novel self-supporting hybrid structure for all-solid-state supercapacitors with a high energy density. *J. Electroanal. Chem.* **2019**, *848*, 113301. [[CrossRef](#)]

39. Pan, J.; Pang, Z.; Wei, T.; Ke, X.; Wei, C.; Cheng, X.; Qin, Z.; Hu, Y.; Wei, C.; Li, F. Functionalization process of coking sludge: Biochar immobilizing with Fe/Co to enhance the wastewater treatment of ozone. *J. Water Process. Eng.* **2023**, *51*, 103434. [[CrossRef](#)]
40. Wu, J.; Li, J.; Owens, G.; Chen, Z. Toward green nano adsorbents and catalysts: Highly active Fe/Mn nanoparticles for enhanced oxidation of oxytetracycline and levofloxacin. *J. Colloid Interface Sci.* **2023**, *632*, 299–310. [[CrossRef](#)] [[PubMed](#)]
41. Sun, Y.; Wang, X.; Du, F.; Niu, J.; Nan, Y.; Pu, J.; Huang, Y.; Hou, B. Fabrication of Z-scheme  $\text{MnFe}_2\text{O}_4@/\text{SiO}_2/\text{TiO}_2$  composite used for 304 stainless steel photocathodic protection. *J. Electroanal. Chem.* **2022**, *923*, 116813. [[CrossRef](#)]
42. Chen, X.; Cai, S.; Yu, E.; Chen, J.; Jia, H.  $\text{MnO}_x/\text{Cr}_2\text{O}_3$  composites prepared by pyrolysis of Cr-MOF precursors containing in situ assembly of  $\text{MnO}_x$  as high stable catalyst for toluene oxidation. *Appl. Surf. Sci.* **2018**, *475*, 312–324. [[CrossRef](#)]

**Disclaimer/Publisher's Note:** The statements, opinions and data contained in all publications are solely those of the individual author(s) and contributor(s) and not of MDPI and/or the editor(s). MDPI and/or the editor(s) disclaim responsibility for any injury to people or property resulting from any ideas, methods, instructions or products referred to in the content.